Structural, magnetic, and electric properties of $La_{0.7}Sr_{0.3}MnO_3/PbZr_xTi_{1-x}O_3$ heterostructures

M. Ziese,[1,a)] A. Setzer,[1] I. Vrejoiu,[2,b)] B. I. Birajdar,[2] B. J. Rodriguez,[2] and D. Hesse[2]
[1]*Division of Superconductivity and Magnetism, University of Leipzig, D-04103 Leipzig, Germany*
[2]*Max Planck Institute of Microstructure Physics, D-06120 Halle, Germany*

(Received 27 May 2008; accepted 19 July 2008; published online 23 September 2008)

Epitaxial $La_{0.7}Sr_{0.3}MnO_3/PbZr_xTi_{1-x}O_3$ multilayers were fabricated by pulsed-laser deposition and studied by structural, magnetic, and electric characterization techniques. Transmission electron microscopy and x-ray diffractometry proved the excellent structural quality of the samples. A high ferroelectric polarization and stable piezoelectric switching were found for the lead zirconate titanate layers, whereas the manganite layers showed bulklike resistivity and magnetoresistance, both attesting to the high quality of the layers. In a detailed study of the magnetic response of the multilayers multiple magnetization switching was observed that was related to the complex strain state. © *2008 American Institute of Physics*. [DOI: 10.1063/1.2980322]

I. INTRODUCTION

Multiferroic materials have attracted intense research interest in recent years[1–5] since these materials present challenges to the understanding of the fundamental nature of magnetoelectric interactions and offer a broad range of application potential and since it is possible nowadays to fabricate high quality films and heterostructures of these materials. Since the saturation values of both magnetization and electric polarization are comparatively small in most intrinsic multiferroics,[2,6] considerable research activity has focused on extrinsic multiferroics, i.e., superlattice systems consisting of alternating ferromagnetic and ferroelectric layers.[7–11] Moreover, in laminates based on Terfenol-D ($Tb_{1-x}Dy_xFe_{2-y}$) and $PbZr_xTi_{1-x}O_3$ very high values of the magnetoelectric coupling constant were found.[12,13] This is in the line of general interest in $PbZr_xTi_{1-x}O_3$ heterostructures since this material has excellent ferroelectric and piezoelectric properties making it of potential use for nonvolatile random access memories.[14,15] An additional degree of versatility of $PbZr_xTi_{1-x}O_3$ lies in the tunability of the lattice parameter and physical properties due to the Zr/Ti composition ratio.[16] Instead of combining $PbZr_xTi_{1-x}O_3$ with metallic ferromagnets, it might be more desirable to fabricate and study heteroepitaxial all-oxide multilayers. Here $La_{0.7}Sr_{0.3}MnO_3$ might be a good choice as ferromagnetic oxide since it has a Curie temperature of about 360 K above room temperature and since it is known to show strong magnetoelastic coupling,[17,18] thus potentially allowing for high magnetoelectric effects mediated via a piezoelectric-magnetoelastic coupling.

In this work the structural, magnetic, and electric properties of $La_{0.7}Sr_{0.3}MnO_3/PbZr_xTi_{1-x}O_3$ multilayers and graded multilayers were investigated and compared with the properties of single $La_{0.7}Sr_{0.3}MnO_3$ (LSMO) films. The focus of this study was the structural and magnetic properties of these heterostructures and here especially the relation between magnetic homogeneity and structural properties.

II. EXPERIMENTAL

Single films, bilayers, and multilayers were fabricated by pulsed-laser deposition (PLD) using a KrF excimer laser ($\lambda = 248$ nm) following the procedure described in Ref. 19 for the growth of single crystalline $PbZr_{0.2}Ti_{0.8}O_3$ thin films. All samples—with the exception of sample VM09 that was grown on (0.1%)Nb-doped $SrTiO_3$ (001)—were deposited onto vicinal single crystalline $SrTiO_3$ (001) (STO) substrates with a miscut angle of about 0.1° (CrysTec, Berlin). Three different classes of samples were produced and investigated, namely, single LSMO films, $LSMO/PbZr_{0.2}Ti_{0.8}O_3$ multilayers and graded $LSMO/PbZr_xTi_{1-x}O_3$ (PZ_xT_{1-x}) heterostructures, where in the latter the Zr/Ti ratio was varied from one PZ_xT_{1-x} layer to the next. The ablation was made from ceramic targets of composition $Pb_{1.1}(Zr_xTi_{1-x})O_3$ ($x = 0.1, 0.15, 0.2, 0.3, 0.4, 0.52$) and $La_{0.7}Sr_{0.3}MnO_3$. The substrate temperature during deposition was 600 °C, oxygen partial pressure was 0.3 mbar; all samples were cooled down in 1 bar O_2 with a cooling rate of 20 °C/min.

Transmission electron microscopy (TEM) investigations were performed on cross-sectional samples (electron beam incident from the [100] STO direction). Conventional TEM was performed in a Philips CM20T electron microscope (200 keV primary energy) and high-resolution TEM (HRTEM) in a Jeol 4010 (at 400 keV). *Z*-contrast imaging was performed in a FEI Titan 80–300 microscope at 300 kV. X-ray diffraction measurements were made with Cu $K\alpha$ radiation using a Philips X'Pert diffractometer. Piezoresponse force microscopy (PFM) was performed using a suitably modified commercially available atomic force microscope (AFM) (ThermoMicroscopes Autoprobe CP-R) with custom tip and sample holders, and PtIr coated tips (Nanosensors, ATEC-EFM) with an elastic constant of about 2.5 N/m. Macroscopic polarization hysteresis curves were acquired using a TF2000 Analyzer (AixaCCT). Magnetic measurements were made with a superconducting quantum interference device

[a)]Electronic mail: ziese@physik.uni-leipzig.de.
[b)]Electronic mail: vrejoiu@mpi-halle.de.

TABLE I. Samples investigated in this work with some basic parameters. n denotes the number of LSMO/PZ_xT_{1-x} bilayers within the heterostructures and T_C the Curie temperature of the ferromagnetic transition. c_{PZT} and c_{LSMO} are the c-axis lattice constants of the PZ_xT_{1-x} and LSMO layers, respectively. In the case of multilayers a LSMO layer is always the first layer grown on the STO substrate. In the case of graded multilayers the bottom PZ_xT_{1-x} layer is the rightmost in the table.

	Description	$(LSMO/PZT)_n$ (nm)	Composition (PZT)	c_{PZT} (nm)	c_{LSMO} (nm)	T_C (K)
VM12	Single layer	$(5/\cdots)_1$	⋯	⋯	⋯	316
VM06	Single layer	$(15/\cdots)_1$	⋯	⋯	0.385	346
VM13	Single layer	$(40/\cdots)_1$	⋯	⋯	0.385	348
VM05	Bilayer	$(70/90)_1$	$PZ_{0.20}T_{0.80}$	⋯	⋯	⋯
VM03	Multilayer	$(10/6)_{15}$	$PZ_{0.20}T_{0.80}$	⋯	⋯	322
VM08	Multilayer	$(6/5)_{15}$	$PZ_{0.20}T_{0.80}$	0.414	0.385	335
VM09	Multilayer	$(9/6)_{15}$	$PZ_{0.20}T_{0.80}$	0.412	0.384	332
VM15	Graded multilayer	$(15/27)_3$	$PZ_{0.52}T_{0.48}/PZ_{0.40}T_{0.60}/PZ_{0.20}T_{0.80}$	⋯	⋯	346
VM16	Graded multilayer	$(9/20)_3$	$PZ_{0.20}T_{0.80}/PZ_{0.15}T_{0.85}/PZ_{0.10}T_{0.90}$	0.410/0.414/0.418	0.384	339
VM17	Graded multilayer	$(11/29)_3$	$PZ_{0.30}T_{0.70}/PZ_{0.20}T_{0.80}/PZ_{0.10}T_{0.90}$	0.412/0.414/0.416	0.385	339
VM24	Graded multilayer	$(20/100)_3$	$PZ_{0.52}T_{0.48}/PZ_{0.30}T_{0.70}/PZ_{0.10}T_{0.90}$	0.412/0.414/0.417	0.384	339

magnetometer (Quantum Design, MPMS7) and an ac-susceptometer (Lakeshore, ACS7000). Resistivity and magnetoresistance were measured in a He flow cryostat (Oxford Instruments) operating in a temperature regime between 4 and 300 K in magnetic fields of up to 9 T. For in-plane resistivity measurements, four contacts were made to the sample using silver paste such as to contact all manganite layers. For out-of-plane current-voltage characterization, Pt contacts were sputtered onto the multilayers as top electrodes and the conducting Nb:STO substrate was used as a bottom contact. All measurements were performed with a four-point method; in the case of the out-of-plane measurements, two contacts each were made to the top layer and substrate back side. In general, magnetic fields were applied along [100] within the heterostructure plane; the magnetization of one sample (VM09) was measured in both in-plane and out-of-plane fields. The diamagnetic contribution of the substrate was determined from the high field magnetization values under the assumption that the ferromagnetic component from the LSMO layers saturates at high field. From all magnetization data the substrate contribution was subtracted. Table I shows an overview of the samples studied in this work.

III. RESULTS AND DISCUSSION

A. Structural characterization

The TEM investigations of our LSMO/PZT bilayers and multilayers revealed their overall high structural quality. Figure 1(a) shows the cross-sectional TEM micrograph of a bilayer of 90 nm thick $PZ_{0.2}T_{0.8}$ grown on 70 nm thick LSMO on a vicinal STO (001) substrate (sample VM05). Figure 1(b) is a cross-sectional HRTEM micrograph taken on a graded LSMO/PZ_xT_{1-x} superlattice with six layers (sample VM17): three layers of 10 nm thin LSMO sandwiched between the STO substrate and three successive layers of PZ_xT_{1-x} (30 nm thin) with increasing x (x=0.1,0.2,0.3). Only the LSMO layers and the first two PZT layers are visible in this micrograph and, as higher magnification images show, the LSMO/PZ_xT_{1-x} interfaces are coherent. Figure 1(c) is a cross-sectional TEM micrograph of a thicker graded LSMO/PZ_xT_{1-x} superlattice with six layers (sample VM24): the three layers of 20 nm thin LSMO being now sandwiched between the STO substrate and the three successive layers of PZ_xT_{1-x} (100 nm thick) with increasing x (x=0.1,0.3,0.5).

A TEM micrograph taken on a LSMO/$PZ_{0.2}T_{0.8}$ multilayer with 30 layers, with 6 nm thin LSMO and 5 nm thin $PZ_{0.2}T_{0.8}$ layers (sample VM08), is shown in Fig. 1(d). The quality of the LSMO/$PZ_{0.2}T_{0.8}$ interfaces in such a multilayer was investigated by means of Z-contrast scanning TEM and it was found that the interfaces are at least partly atomically flat and coherent [see inset in Fig. 1(d)].

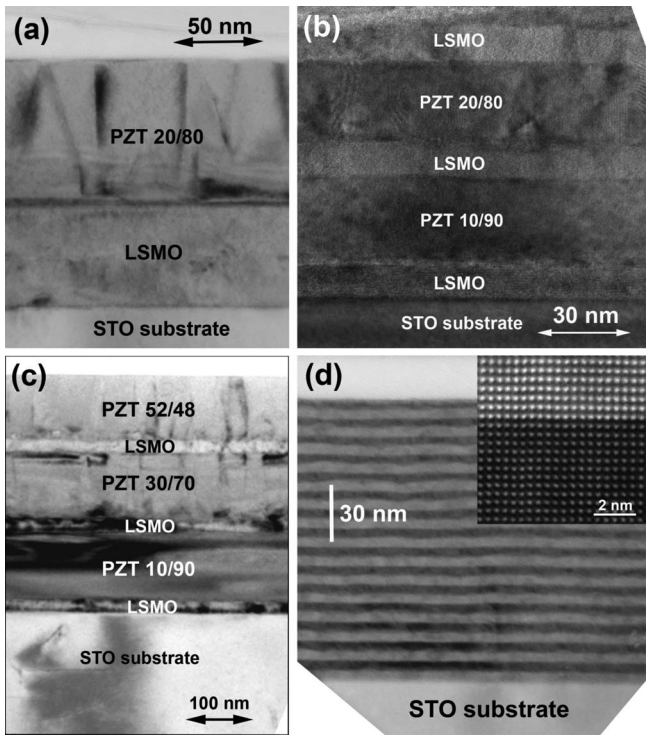

FIG. 1. Cross sectional TEM and HRTEM micrographs of LSMO/PZ_xT_{1-x} bilayers and multilayers: (a) a 70 nm thin LSMO/90 nm thin $PZ_{0.2}T_{0.8}$ bilayer (sample VM05), (b) a graded LSMO/PZ_xT_{1-x} multilayer (VM17) with six layers (x=0.1,0.2,0.3), (c) a graded LSMO/PZ_xT_{1-x} multilayer (VM24) with six layers (x=0.1,0.3,0.52), and (d) a multilayer (VM08) with 15 LSMO/$PZ_{0.2}T_{0.8}$ bilayers (bright contrast are LSMO and dark contrast are $PZ_{0.2}T_{0.8}$ layers). The inset in (d) shows a Z-contrast STEM of a LSMO/$PZ_{0.2}T_{0.8}$ interface in such a multilayer (bright contrast PZT, dark contrast LSMO).

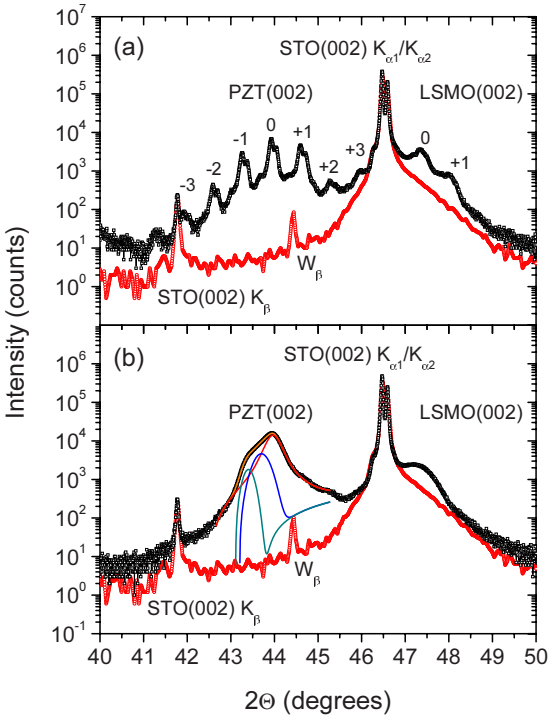

FIG. 2. (Color online) Θ-2Θ scans of samples (a) VM09 and (b) VM24 around the (002) substrate reflection. The lower curves in each figure show the corresponding scan for a virgin $SrTiO_3$ (001) substrate. In (a) satellite peaks due to the superlattice modulation are clearly seen especially for the $PZ_{0.2}T_{0.8}$ (002) reflection and are indexed by their order $0, \pm 1, \ldots$. In (b) a broad PZ_xT_{1-x} (002) reflection appears. The solid lines in (b) indicate the peak-profile analysis of this reflection by three peaks corresponding to the three PZ_xT_{1-x} layers.

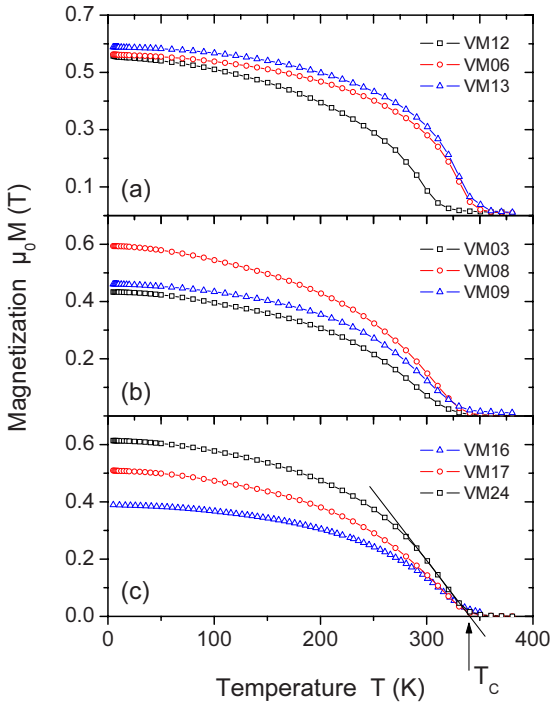

FIG. 3. (Color online) Magnetization as a function of temperature of (a) single LSMO films, (b) $LSMO/PZ_{0.2}T_{0.8}$ multilayers, and (c) graded $LSMO/PZ_xT_{1-x}$ heterostructures. The magnetization was measured in an in-plane field of 0.2 T along [100]. The diamagnetic contribution from the substrate was subtracted. The Curie temperature was determined by linear extrapolation of the magnetization to the base line as indicated in (c).

Figure 2 shows Θ-2Θ scans of multilayer VM09 and the graded multilayer VM24 near the (002) reflection. In the case of multilayer VM09 containing 15 bilayers with thickness of 15 nm, clear satellite peaks due to the superlattice modulation were observed. These were indexed according to their order, $n=0, \pm 1, \ldots$. Four of these reflections show a clear $K_{\alpha1}/K_{\alpha2}$ splitting. These observations attest to the high quality of the multilayer. From the central peak a *c*-axis lattice constant of 0.412 nm was derived for the PZT layers. From the satellite shifts the superlattice modulation period was obtained to 14–15 nm. For multilayer VM08 a similar analysis yielded a modulation period of 11–12 nm. Both values are in good agreement with the TEM results. Near the LSMO (002) reflection only one satellite peak was observed. The *c*-axis lattice constant of LSMO was derived as 0.384 nm and the superlattice modulation period from the first order satellite reflection as 15 nm. The graded multilayers showed a distinctly different intensity pattern [see Fig. 2(b)]. In this case superstructure modulations were not observed since there were only three bilayers; instead, the PZ_xT_{1-x} (002) reflection was found to be very broad due to the compositional variation from one to the next PZ_xT_{1-x} layer. To obtain an estimate of the *c*-axis lattice constants of the PZ_xT_{1-x} layers the peak profiles of the corresponding (002) reflections were analyzed by fitting three pseudo-Voigt functions to the intensity profile in the angle range between 42.6° and 45.2° [see Fig. 2(b)]. From the positions of the maxima the *c*-axis lattice constants were calculated and were found to be between 0.410 and 0.418 nm (see Table I).

B. Magnetic properties

1. Overview

In order to obtain a first overview of the magnetic properties, the magnetization was measured as a function of temperature in an in-plane field of 0.2 T that brings the samples into technical saturation. Figure 3 shows the respective magnetization data for the (a) single films, (b) multilayers, and (c) graded multilayers. The volume of the LSMO layers needed to calculate the magnetization was determined from the sample area and the layer thickness is measured either by cross-sectional TEM or estimated from the deposition time. The LSMO volume therefore has a considerable error of at least 10%; this error is especially large in the multilayer samples since the error in the thickness determination of a single LSMO layer is multiplied by the number of bilayers. Therefore the scatter in the saturation magnetization $M_S(0)$ is significantly larger for the multilayers than for the thin films. Apart from this scatter the values of the saturation magnetization are consistently below the theoretical spin-only magnetic moment that is 3.7 μ_B/unit cell for $La_{0.7}Sr_{0.3}MnO_3$; this corresponds to $\mu_0 M_S = 0.75$ T. This might be caused by various effects, namely, a high field slope of the magnetization[20] as well as spin disorder,[21] orbital ordering,[22,23] phase separation,[24,25] or structural inhomogeneity[26,27] at the interfaces. The Curie temperature is often determined from the inflection point of the magnetization versus temperature curve.[28] This approach does not yield sensible results here since the magnetization curves of the multilayers are broadened. Therefore the Curie temperature was determined by linear extrapolation of the high tem-

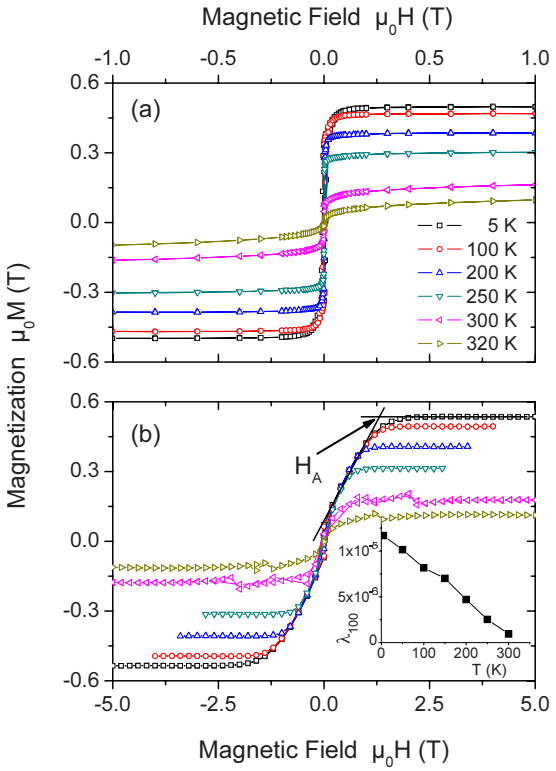

FIG. 4. (Color online) Magnetization vs applied field of sample VM09 for (a) in-plane [100] and (b) out-of-plane [001] orientation of the magnetic field. The solid lines in (b) indicate the construction used for the determination of the anisotropy field H_A. The diamagnetic contribution from the substrate was subtracted. The inset in (b) shows the saturation magnetostriction λ_{100} as determined from the anisotropy field as a function of temperature.

perature magnetization tail onto the base line [see Fig. 3(c)]. The corresponding Curie temperature values are listed in Table I.

2. Magnetic anisotropy and magnetostriction

The magnetization of multilayer VM09 was measured in in-plane and out-of-plane magnetic fields to assess the anisotropy (see Fig. 4). The out-of-plane direction is obviously the hard axis.[29,30] From the out-of-plane measurements the anisotropy field H_A was determined as shown in Fig. 4(b). The anisotropy field is related to shape anisotropy, the magnetocrystalline anisotropy constant K_1 of the undistorted LSMO layers, and to a strain-induced anisotropy term due to magnetostriction[30]

$$\mu_0 H_A = \mu_0 M_S + \frac{2K_1}{M_S} + \frac{3\lambda_{100}}{M_S}(c_{11} - c_{12})(1 + 2c_{12}/c_{11})\epsilon. \tag{1}$$

For the derivation of this formula a coherently strained LSMO film with biaxial strain components $\epsilon_{xx} = \epsilon_{yy} = \epsilon$ was assumed. λ_{100} denotes the saturation magnetostriction and c_{11} and c_{12} are elastic constants of the LSMO layer.

From the magnetization data the anisotropy field and saturation magnetization were determined between 10 and 300 K with values of $\mu_0 H_A$ ranging between 1.37 and 0.38 T and of $\mu_0 M_S$ between 0.54 and 0.18 T, respectively. The magnetocrystalline anisotropy constant K_1 is known to be negative and comparatively small[30] with $|K_1| < 4$ kJ/m^3 such that $2|K_1|/M_S < 2 \times 10^{-5}$ T, which is negligible in comparison to the anisotropy field $\mu_0 H_A$ and saturation magnetization $\mu_0 M_S$. The fact that the anisotropy field has more than twice the value of the saturation magnetization shows that the strain dependent anisotropy is large. The saturation magnetostriction λ_{100} can be directly calculated from the measured values of H_A and M_S using Eq. (1) and the values for the strain ϵ and the elastic constants c_{11} and c_{12}, in good approximation for LSMO $c_{11} \simeq 2c_{12} \simeq 200$ GPa.[31] The strain $\epsilon = 0.02$ was calculated from the bulk lattice constants of 0.3875 nm (LSMO) and 0.3954 nm ($PZ_{0.2}T_{0.8}$). This yields the saturation magnetostriction λ_{100} shown in the inset in Fig. 4(b). λ_{100} was found to decrease linearly with temperature, extrapolating to zero at 326 K in reasonable agreement with the Curie temperature of this film of 332 K. The values of λ_{100} obtained here are consistent with the values obtained from Ref. 30 for a 130 nm thick LSMO film.

3. Strain dependence of the coercive field

It is well known that the coercive field depends sensitively on strain through a stress-induced anisotropy.[32] A manifestation of this effect can be beautifully seen in manganite films grown on $SrTiO_3$ substrates. Below the structural transition of $SrTiO_3$ at about 105 K crystallographic domains form and induce elastic deformations in the manganite film which, in turn, lead to the appearance of three branches of the coercive field.[33,34] This effect is also seen in one of the multilayers studied here and will be further discussed below. Another possibility to modify the coercive field is by inducing different strains in the individual LSMO layers of a multilayer sample. To this end, graded multilayers consisting of LSMO layers sandwiched between PZT layers with various compositions were grown. With increasing Zr/Ti ratio the PZT layers have larger in-plane lattice parameters [$a(PZ_{0.1}T_{0.9}) = 0.3927$ nm, $a(PZ_{0.2}T_{0.8}) = 0.3954$ nm, $a(PZ_{0.3}T_{0.7}) = 0.3978$ nm, and $a(PZ_{0.52}T_{0.48}) = 0.4046$ nm, bulk room temperature values], all larger than a(LSMO) $= 0.3875$ nm (pseudocubic) and a(STO) $= 0.3905$ nm.

Figure 5(a) shows the magnetization hysteresis loops of sample VM17 at various temperatures. At 5 and 100 K stepped hysteresis curves are clearly seen,[11] i.e., at these temperatures the magnetization measurements clearly show two coercive fields. Since there are three layers present in each graded heterostructure, one would expect to observe three magnetization reversal steps. For an accurate determination of the coercive fields, the field derivative of the magnetization was computed [see Fig. 5(b)]. In case of this sample, the derivative actually indicates that there are four magnetization reversal steps in total, with two each being arranged in a double transition. For samples VM16 and VM24 at 5 K indeed three coercive fields are observed, where in each case two transitions are very close. At higher temperatures it is even more difficult to resolve the separate magnetization switching by magnetization measurements. Therefore measurements of the fundamental ac susceptibility

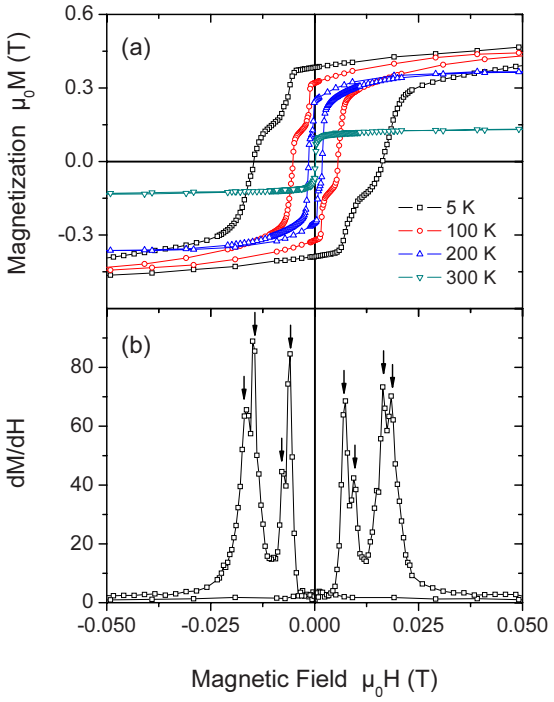

FIG. 5. (Color online) (a) Magnetization hysteresis loops of sample VM17 measured in an in-plane field along [100] for various temperatures. (b) Field derivative dM/dH of the magnetization curve at 5 K. The arrows mark the coercive field values.

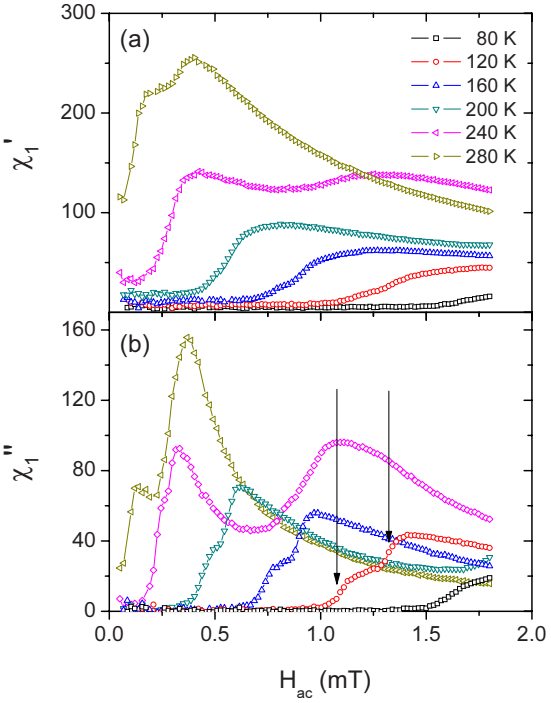

FIG. 6. (Color online) (a) In-phase and (b) quadrature component of the fundamental ac susceptibility of the graded multilayer VM17 as a function of the ac-field amplitude for various temperatures. As indicated in (b) for the 120 K data the transitions in the loss component were used to determine the coercive fields.

$$\chi_1' - i\chi_1'' = \frac{1}{\pi H_{\mathrm{ac}}} \int_0^{2\pi} M(t)\exp(-i\omega t)d(\omega t) \qquad (2)$$

were performed with a fixed frequency $\omega/(2\pi)=667$ Hz as a function of the ac-field amplitude H_{ac}. Figure 6 shows the ac susceptibility of sample VM17 at various temperatures. At a coercive field the loss component χ_1'' shows a clear transition[35] that was used for the determination of the coercive field values. The results are summarized in Fig. 7. In the case of the magnetization measurements the coercive fields were calculated as averages between positive and negative field values. In all cases there is reasonable agreement between the coercive field values determined by the two techniques. In sample VM16 indeed three coercive fields were found for all temperatures: in sample VM17 the three coercive fields at high temperatures split up into four at low temperatures and in sample VM24 apart from 5 K only two magnetization reversals were detected.

It is impossible to assign the magnetic transitions to particular layers but it is likely that the LSMO layer adjacent to the STO substrate has the smallest coercive field since it is the least strained. The origin of the additional transitions in sample VM17 might either be due to structural inhomogeneities or to the fact that each LSMO layer is sandwiched between layers of different lattice constants. This might lead to an inhomogeneous strain distribution within the LSMO layer (see Refs. 36 and 37). Although this is true for all graded multilayers, the actual strain distribution within the multilayers will be different in each case since the thickness of the PZT layers was varied from sample to sample. The PZT layers in sample VM24 were especially thick (100 nm) and one might assume that strain relaxation has already set in such that the strain state of the two upper LSMO layers is similar; this would explain the absence of the third magnetization reversal step in this sample in a broad temperature range. Since strain relaxation is accompanied by the formation of misfit dislocations that might act as pinning centers

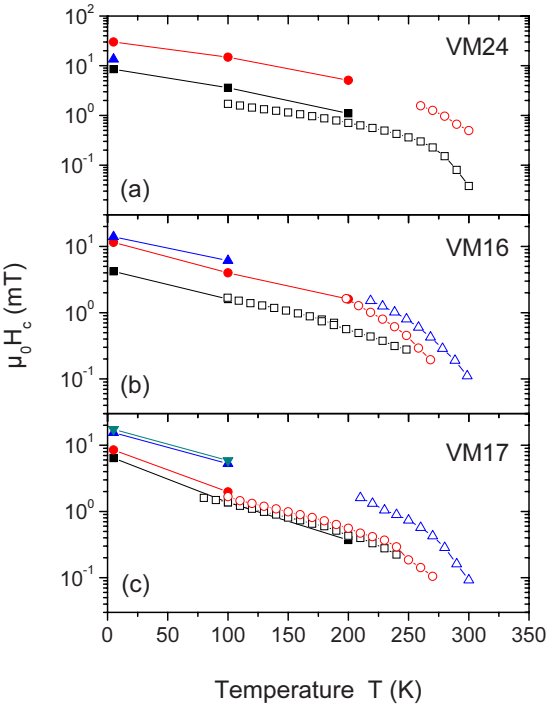

FIG. 7. (Color online) Coercive fields determined from magnetization (solid symbols) and ac-susceptibility (open symbols) measurements of the graded heterostructures (a) VM24, (b) VM16, and (c) VM17.

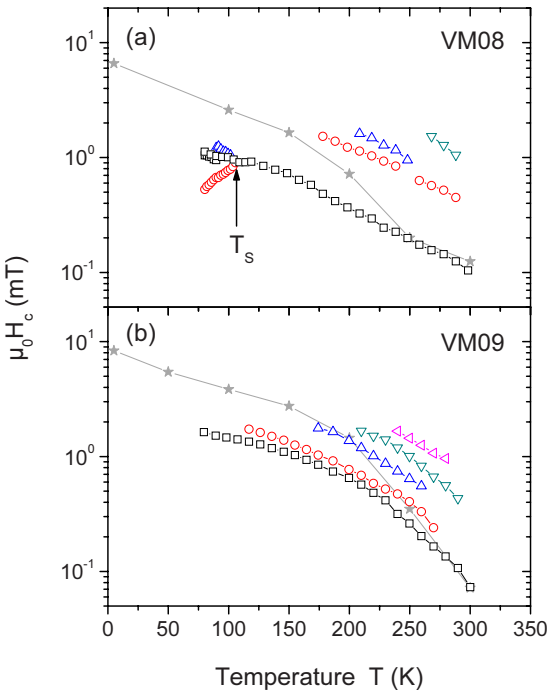

FIG. 8. (Color online) Coercive fields determined from magnetization (stars) and ac-susceptibility (open symbols) measurements of the multilayers (a) VM08 and (b) VM09. In (a) T_S denotes the temperature of the structural transition in the $SrTiO_3$ substrate.

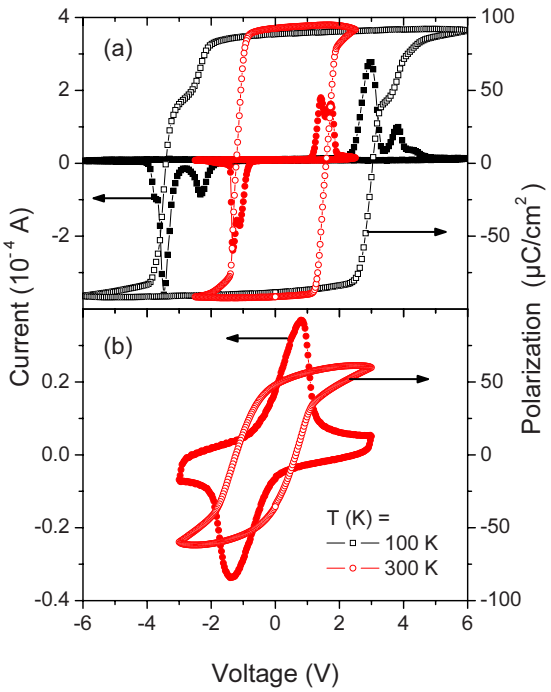

FIG. 9. (Color online) Ferroelectric hysteresis loops measured on (a) a $LSMO/PZ_{0.2}T_{0.8}$ bilayer (VM05) and (b) a graded $LSMO/PZ_xT_{1-x}$ heterostructure with six layers (x=0.1,0.3,0.52) (VM24). Right axis shows the electric polarization, left axis shows the current.

for magnetic domain walls, one might expect that sample VM24 has larger coercive fields than samples VM16 and VM17. This is indeed observed.

That strain relaxation might have some effect on the coercive field is further seen in the analysis of the magnetic data of the multilayers VM08 and VM09. Although only a single magnetization reversal is observed in the magnetization hysteresis [see Fig. 4(a)], high-resolution ac-susceptibility measurements reveal magnetic inhomogeneity. The coercive fields were again determined from the loss component χ_1'' and are presented in Fig. 8. In these two samples at high temperature, four to five coercive fields were observed. This might be related to strain relaxation throughout the multilayer leading to different strain states of the individual LSMO layers. Although strain relaxation could not be verified by the Θ-2Θ scans, we would expect strain relaxation to occur in multilayers with a thickness exceeding 100 nm. Furthermore in the case of sample VM08 the influence of the structural transition of the STO substrate at 105 K on the magnetic properties was observed. Below 105 K the lowest lying coercive field splits up into three branches corresponding to the three orientations of the tetragonal cell of the STO substrate with respect to the ac-field amplitude. This transition is also seen in the single LSMO films and was discussed in a separate publication.[33] We would believe that this transition also occurs in sample VM09 and in the higher lying coercivity branches. We can, however, not observe this since the ac susceptometer has a maximum ac-field amplitude of 1.8 mT.

In summary, strain effects in the multilayers have a strong influence on the magnetic properties. This is manifested in a large perpendicular anisotropy and in the appearance of stepped magnetization curves related to the appearance of multiple coercive field branches.

C. Electric properties

1. Ferroelectric polarization

Ferroelectric measurements performed on the $LSMO/PZ_{0.2}T_{0.8}$ bilayer (sample VM05) shown in Fig. 9(a) confirmed the good structural quality of the sample. Hysteresis loops measured at temperatures of 100 and 300 K and at 1 kHz are given in Fig. 9(a). The remnant polarization was almost temperature insensitive up to 300 K, being about $P_r = 88 \pm 10\ \mu C/cm^2$, comparable with polarization values obtained for single crystalline $PZ_{0.2}T_{0.8}$ films grown on $SrRuO_3$-coated STO (100).[19] The double transition evidenced by the two current peaks in the current-voltage curves and the two steps of the polarization-voltage curves in Fig. 9(a) may arise from the existence of two types of 180° domains in the PZT layer, whose polarization switching at low temperature occurs at different values of the applied voltage.

The ferroelectric hysteresis loop measured at 300 K and at 1 kHz on the graded sample VM24, whose TEM image is given in Fig. 1(c), is plotted in Fig. 9(b). The measured remnant polarization is $P_r = 45 \pm 10\ \mu C/cm^2$. This is most probably solely the contribution of the topmost 100 nm thick $PZ_{0.52}T_{0.48}$ layer of the six-layered structure because the three LSMO layers are in contact on the sides of the substrate and thus short circuited.[11] The value of the remnant polarization is also close to what $PZ_{0.52}T_{0.48}$ is expected to have, $P_r = 50\ \mu C/cm^2$.[38]

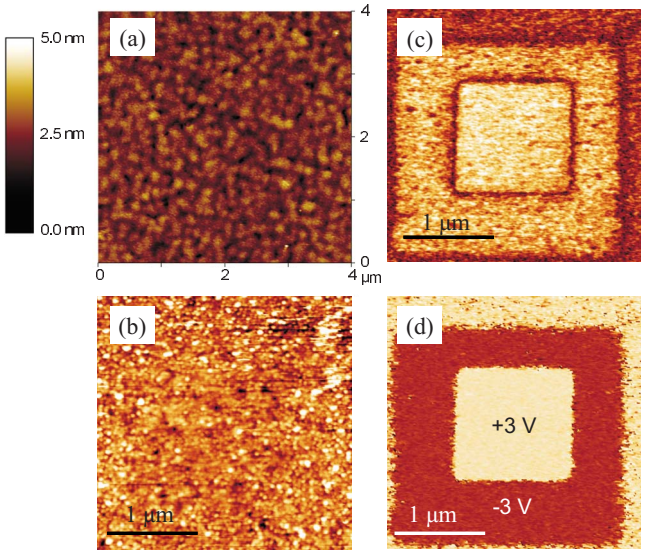

FIG. 10. (Color online) (a) AFM (tapping mode) topography, (b) contact mode topography, (c) PFM amplitude image (giving information about the out-of-plane polarization magnitude), and (d) PFM phase image (giving information about the out-of-plane polarization direction) acquired on the top surface of a multilayer with 15 LSMO/$PZ_{0.2}T_{0.8}$ bilayers (VM09) grown on Nb:STO (001). The structures visible in (c) and (d) were written before imaging by applying voltages of +3 and −3 V between tip and sample, respectively.

2. PFM

PFM (Ref. 39) investigations were performed on a LSMO/$PZ_{0.2}T_{0.8}$ multilayer with 30 layers (9 nm thin LSMO layers and 6 nm thin $PZ_{0.2}T_{0.8}$ layers) grown on conductive Nb:STO (001) (sample VM09). Part of the sample was cut by a diamond saw so that the sides of the substrate that had been covered by material during the PLD fabrication were removed to avoid the LSMO layers being short circuited. Figure 10(a) shows an AFM topography image obtained in a tapping mode on a 4×4 μm^2 area of the as-grown top surface of this multilayer and Fig. 10(b) is a topography image (2.5×2.5 μm^2 area) obtained in a contact mode after the sample was cut. The out-of-plane piezoresponse images associated with the topography image shown in Fig. 10(b) are given by the PFM amplitude image in Fig. 10(c) and the PFM phase image in Fig. 10(d). The orientation of the polarization of the topmost 6 nm thin $PZ_{0.2}T_{0.8}$ layer could be switched by applying a dc voltage of either +3 or −3 V during scanning, as shown in Fig. 10(d), and these two polarization states were stable in time (no backswitching occurred). From earlier investigations, our epitaxial $PZ_{0.2}T_{0.8}$ films (thinner than $\simeq$90 nm) grow fully *c*-axis oriented and show uniform orientation of the polarization in the as-grown state, as demonstrated in a previous paper (Ref. 19).

3. Current-in-plane resistivity and magnetoresistance

The current-in-plane resistivity of multilayer VM08 was measured as a function of temperature and magnetic field (see Fig. 11). The data are unusual in the sense that the resistivity and magnetoresistance are not significantly modified as compared to single manganite films.[28,40] Magnetotransport measurements are a sensitive probe for structural defects since these lead to both an upturn in the resistivity at low temperatures and the appearance of a considerable low field magnetoresistance.[41] None of these signatures are seen in the multilayer, thus corroborating the excellent structural quality.

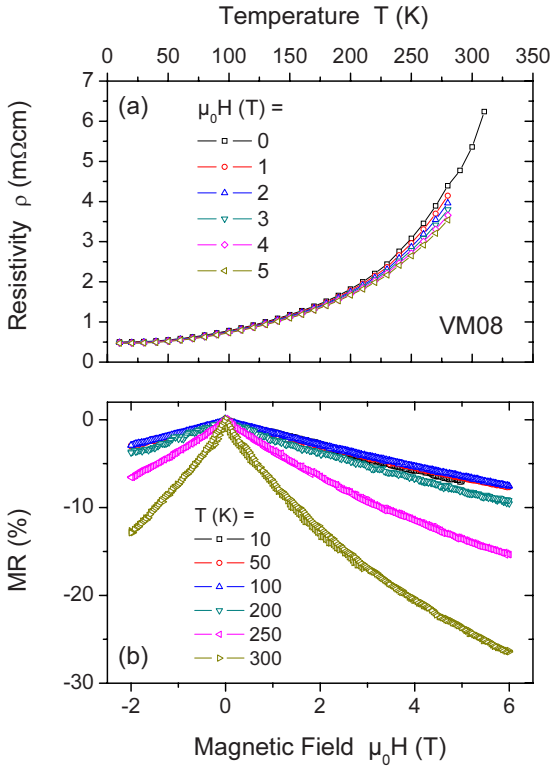

FIG. 11. (Color online) (a) In-plane resistivity of multilayer VM08 as a function of temperature for various magnetic fields. (b) Magnetoresistance of multilayer VM08 as a function of magnetic field at various temperatures. Note that the 10 and 50 K data are hidden by the 100 K data.

4. Current-perpendicular-to-plane transport

The current-voltage characteristics of multilayer VM09 were measured in a current-perpendicular-to-plane configuration. For this platinum contacts on the top PZT layer and the conducting Nb-doped $SrTiO_3$ substrate were used as electrodes. Polarity of the voltage was such that forward bias corresponded to a positive voltage applied to the platinum contacts. Figure 12 shows selected current-voltage (*I-V*) characteristics as well as the dynamic conductance dI/dV derived from these at 10 and 300 K. Main features of the data are the rectifying characteristics of the current-voltage characteristics and the exponential voltage dependence of the current and dynamic conductance for forward bias. The magnetic field dependence is weak, especially in the forward bias region. The data do not show any irreversibility related to a switching of the PZT layers.

A comparison of these data with literature data on the rectifying behavior at the $La_{0.7}Sr_{0.3}MnO_3$– and $La_{0.7}Ca_{0.3}MnO_3$–Nb:$SrTiO_3$ interface shows essentially the same behavior.[42,43] Therefore we suspect that the PZT layers are short circuited by edge defects such that the current-voltage characteristics are dominated by the LSMO/STO interface. The rectifying behavior is due to the formation of a *p-n*-junction between the *n*-doped Nb:$SrTiO_3$ and the

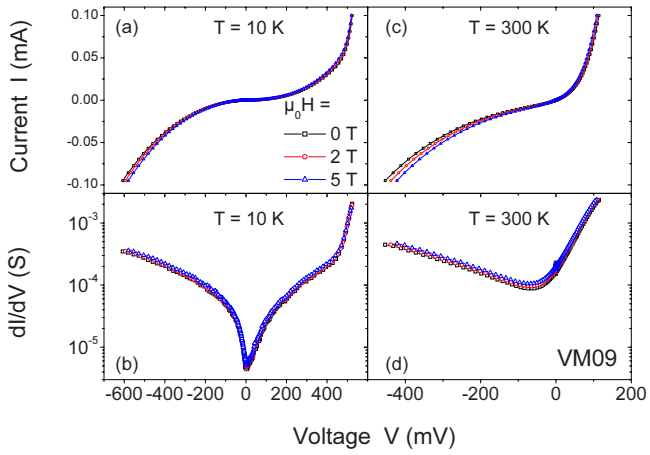

FIG. 12. (Color online) Perpendicular-to-plane current-voltage characteristics at (a) 10 K and (c) 300 K as well as dynamic conductance at (b) 10 K and (d) 300 K of the multilayer VM09. All measurements were performed in magnetic fields of 0, 2, and 5 T.

p-doped LSMO. The magnetoresistance is sometimes believed to be due to a shift of the chemical potential in the LSMO under the action of a magnetic field.[44] However, since the voltage dependence of the magnetoresistance is not particularly strong in multilayer VM09 (not shown), it is more likely that the magnetoresistance is caused by the intrinsic magnetoresistance of the LSMO layers.

IV. CONCLUSIONS

In this work the structural, electric, and magnetic properties of LSMO single films, LSMO/PZT bilayers, LSMO/PZT superlattices, and LSMO/PZ_xT_{1-x} graded multilayers fabricated by PLD were studied. TEM and x-ray diffractometry measurements showed heteroepitaxial growth with well-defined flat and coherent interfaces. Measurements of the current-in-plane resistivity and magnetoresistance reflect the properties of the LSMO layers exclusively. Here the absence of both a low temperature upturn in the resistivity and a low temperature low field magnetoresistance clearly show that the LSMO layers have single crystalline quality. The behavior of the current-perpendicular-to-plane current-voltage characteristics is dominated by the formation of a *pn*-junction at the interface between LSMO and the Nb-doped $SrTiO_3$ substrate since the LSMO layers in the superlattice are short circuited by edge defects and bridge the PZT layers. For the same reason, the ferroelectric polarization and piezoelectric response are dominated by the topmost PZT layer. Stable electric switching was found with remnant polarization in agreement with results on single layers. The magnetic characterization revealed multiple magnetization switching. This was interpreted as arising from the reversal of individual LSMO layers in the graded multilayers due to modifications of the coercive fields of these layers by the differential strain exerted by the adjacent PZ_xT_{1-x} layers. The mechanism leading to magnetic inhomogeneity in the superlattices is less obvious but probably related to strain relaxation.

From the data presented here we conclude that the multilayers are of excellent structural, ferromagnetic, and ferroelectric quality. In further studies the magnetoelectric coupling between PZT and LSMO layers will be investigated. To this end the multilayers will be etched into pillars that will be separately contacted to both avoid the problem of short circuiting and enable the study of size effects.

ACKNOWLEDGMENTS

This work was supported by the DFG within the Collaborative Research Center SFB 762 "Functionality of Oxide Interfaces." One of the authors (B.J.R.) also acknowledges the support of the Alexander von Humboldt Foundation. We thank Dr. E. Pippel for the STEM *Z*-contrast image, Dr. A. Lotnyk for the HRTEM micrograph, Dr. L. Pintilie for the measurements shown in Fig. 9(a), and Dr. M. Alexe for fruitful discussions.

[1] N. A. Hill, J. Phys. Chem. B **104**, 6694 (2000).
[2] M. Fiebig, J. Phys. D **38**, R123 (2005).
[3] K. Dörr and C. Thiele, Phys. Status Solidi B **243**, 21 (2006).
[4] R. Ramesh and N. A. Spaldin, Nat. Mater. **6**, 21 (2007).
[5] W. Eerenstein, N. D. Mathur, and J. F. Scott, Nature (London) **442**, 759 (2006).
[6] D. I. Khomskii, J. Magn. Magn. Mater. **306**, 1 (2006).
[7] A. R. Chaudhuri, R. Ranjith, S. B. Krupanidhi, R. V. K. Mangalam, A. Sundaresan, S. Majumdar, and S. K. Ray, J. Appl. Phys. **101**, 114104 (2007).
[8] P. Murugavel, M. P. Singh, W. Prellier, B. Mercey, C. Simon, and B. Raveau, J. Appl. Phys. **97**, 103914 (2005).
[9] W. Prellier, M. P. Singh, and P. Murugavel, J. Phys.: Condens. Matter **17**, R803 (2005).
[10] P. Murugavel, P. Padhan, and W. Prellier, J. Phys.: Condens. Matter **18**, 3377 (2006).
[11] I. Vrejoiu, M. Ziese, A. Setzer, P. Esquinazi, B. I. Birajdar, A. Lotnyk, M. Alexe, and D. Hesse, Appl. Phys. Lett. **92**, 152506 (2008).
[12] S. Dong, J. F. Li, D. Viehland, J. Cheng, and L. E. Cross, Appl. Phys. Lett. **85**, 3534 (2004).
[13] C.-W. Nan, M. I. Bichurin, S. Dong, D. Viehland, and G. Srinivasan, J. Appl. Phys. **103**, 031101 (2008).
[14] J. F. Scott and C. A. P. D. Araujo, Science **246**, 1400 (1989).
[15] M. Dawber, K. M. Rabe, and J. F. Scott, Rev. Mod. Phys. **77**, 1083 (2005).
[16] E. Sawaguchi, J. Phys. Soc. Jpn. **8**, 615 (1953).
[17] M. K. Lee, T. K. Nath, C. B. Eom, M. C. Smoak, and F. Tsui, Appl. Phys. Lett. **77**, 3547 (2000).
[18] W. Eerenstein, M. Wiora, J. L. Prieto, J. F. Scott, and N. D. Mathur, Nat. Mater. **6**, 348 (2007).
[19] I. Vrejoiu, G. Le Rhun, L. Pintilie, D. Hesse, M. Alexe, and U. Gösele, Adv. Mater. (Weinheim, Ger.) **18**, 1657 (2006).
[20] J. M. D. Coey, M. Viret, and S. von Molnár, Adv. Phys. **48**, 167 (1999).
[21] M. G. Blamire, B. S. Teo, J. H. Durrell, N. D. Mathur, Z. H. Barber, J. L. MacManus Driscoll, L. F. Cohen, and J. E. Evetts, J. Magn. Magn. Mater. **191**, 359 (1999).
[22] M. Ziese, H. C. Semmelhack, and K. H. Han, Phys. Rev. B **68**, 134444 (2003).
[23] L. Abad, V. Laukhin, S. Valencia, A. Gaup, W. Gudat, L. Balcells, and B. Martínez, Adv. Funct. Mater. **17**, 3918 (2007).
[24] M. H. Jo, N. D. Mathur, N. K. Todd, and M. G. Blamire, Phys. Rev. B **61**, R14905 (2000).
[25] M. Bibes, L. Balcells, S. Valencia, J. Fontcuberta, M. Wojcik, E. Jedryka, and S. Nadolski, Phys. Rev. Lett. **87**, 067210 (2001).
[26] J.-H. Park, E. Vescovo, H.-J. Kim, C. Kwon, R. Ramesh, and T. Venkatesan, Phys. Rev. Lett. **81**, 1953 (1998).
[27] T. Becker, C. Streng, Y. Luo, V. Moshnyaga, B. Damaschke, N. Shannon, and K. Samwer, Phys. Rev. Lett. **89**, 237203 (2002).
[28] M. Ziese, H. C. Semmelhack, K. H. Han, S. P. Sena, and H. J. Blythe, J. Appl. Phys. **91**, 9930 (2002).
[29] J. O'Donnell, M. S. Rzchowski, J. N. Eckstein, and I. Bozovic, Appl. Phys. Lett. **72**, 1775 (1998).
[30] M. Ziese, H. C. Semmelhack, and P. Busch, J. Magn. Magn. Mater. **246**, 327 (2002).
[31] T. W. Darling, A. Migliori, E. G. Moshopoulou, S. A. Trugman, J. J.

Neumeier, J. L. Sarrao, A. R. Bishop, and J. D. Thompson, Phys. Rev. B **57**, 5093 (1998).
[32]S. Chikazumi, *Physics of Ferromagnetism* (Clarendon, Oxford, 1997).
[33]M. Ziese, A. Setzer, I. Vrejoiu, A. Lotnyk, and D. Hesse, New J. Phys. **10**, 063024 (2008).
[34]V. K. Vlasko-Vlasov, Y. K. Lin, D. J. Miller, U. Welp, G. W. Crabtree, and V. I. Nikitenko, Phys. Rev. Lett. **84**, 2239 (2000).
[35]S. Prüfer and M. Ziese, Phys. Status Solidi B **245**, 1661 (2008).
[36]T. K. Nath, R. A. Rao, D. Lavric, C. B. Eom, L. Wu, and F. Tsui, Appl. Phys. Lett. **74**, 1615 (1999).
[37]F. Tsui, M. C. Smoak, T. K. Nath, and C. Eom, Appl. Phys. Lett. **76**, 2421 (2000).
[38]I. Vrejoiu, Y. L. Zhu, G. Le Rhun, M. A. Schubert, D. Hesse, and M. Alexe, Appl. Phys. Lett. **90**, 072909 (2007).
[39]A. Gruverman, O. Auciello, and H. Tokumoto, Annu. Rev. Mater. Sci. **28**, 101 (1998).
[40]M. Bibes, M.-J. Casanove, L. Balcells, S. Valencia, B. Martínez, J.-C. Ousset, and J. Fontcuberta, Appl. Surf. Sci. **188**, 202 (2002).
[41]M. Ziese, Rep. Prog. Phys. **65**, 143 (2002).
[42]H. Tanaka, J. Zhang, and T. Kawai, Phys. Rev. Lett. **88**, 027204 (2002).
[43]D. J. Wang, J. R. Sun, Y. W. Xie, W. M. Lú, S. Liang, T. Y. Zhao, and B. G. Shen, Appl. Phys. Lett. **91**, 062503 (2007).
[44]N. Nakagawa, M. Asai, Y. Mukunoki, T. Susaki, and H. Y. Hwang, Appl. Phys. Lett. **86**, 082504 (2005).